

## A simplified aerosol retrieval algorithm for Himawari-8 Advanced Himawari Imager over Beijing

Zhaoyang Zhang<sup>a,\*</sup>, Meng Fan<sup>b</sup>, Weiling Wu<sup>c</sup>, Zifeng Wang<sup>c</sup>, Minghui Tao<sup>d</sup>, Jing Wei<sup>e</sup>,  
Quan Wang<sup>f,\*\*</sup>

<sup>a</sup> College of Geography and Environmental Sciences, Zhejiang Normal University, Zhejiang Province, China

<sup>b</sup> State Key Laboratory of Remote Sensing Science, Institute of Remote Sensing and Digital Earth, Chinese Academy of Sciences, Beijing, China

<sup>c</sup> Chinese Academy for Environmental Planning, Beijing, China

<sup>d</sup> School of Earth Sciences, China University of Geosciences, Wuhan, China

<sup>e</sup> State Key Laboratory of Earth Surface Processes and Resource Ecology, College of Global Change and Earth System Science, Beijing Normal University, Beijing, China

<sup>f</sup> Faculty of Agriculture, Shizuoka University, Shizuoka, Japan

### ARTICLE INFO

#### Keywords:

Aerosol Optical Depth  
AERONET  
Himawari-8  
High temporal

### ABSTRACT

High temporal aerosol optical depth (AOD) is useful for inverting modelling of emissions and for comprehensively understanding the climatology of aerosol. Geostationary satellite has been used to derive AOD over land and ocean. In this study, a novel simplified aerosol retrieval algorithm for Advanced Himawari-8 imager (SARAH) is developed to retrieve hourly AOD over Beijing from a new-generation geostationary meteorological satellite—Himawari-8, which carries the Advanced Himawari Imager (AHI). The algorithm is based on a simplified radiative transfer model and surface reflectance derived from one-month AHI apparent data. Measurements from Aerosol RObotic NETwork (AERONET) sites and JAXA Himawari Monitor Version 2.0 Aerosol Retrieval product (L2ARP2.0) are used to evaluate the performance of AOD retrievals from SARAH algorithm. There are 73.5%, 78.2%, 74.7% of AOD retrievals falling in the Expected error lines at Beijing CAMS, Beijing\_RADI, and Xianghe sites, respectively. The correlation coefficient is larger than 0.92 with small root mean square error (RMSE) of 0.134–0.164. The retrievals can also reflect the temporal variations of AOD very well. The results indicate that the SARAH AOD algorithm can derive the regional AOD accurately and is better than the L2ARP2.0 AOD.

### 1. Introduction

Atmospheric aerosols consist of particles with different composition, optical properties, and shapes in atmosphere (Hinds, 1999). It has large influences on human health. For example, World Health Organization (WHO) reported that hospital admission increments due to respiratory problems are associated with a rapidly increase of PM mass concentrations in a short period (WHO, 2005). Many studies have also shown the relations between increased PM<sub>2.5</sub> concentrations and adverse health effects in U.S. cities (Schwartz and Neas, 2000; Pope et al., 2009; Chen et al., 2012). Aerosols can also reduce visibility and affect the environment (Zhang et al., 2016a). Until now, the uncertainty of aerosol radiative forcing is still one of the largest uncertainties in climate studies (Field et al., 2014).

Aerosol optical depth (AOD) is the fundamental aerosol optical

property, which can quantify the aerosol loadings in atmosphere. AOD can be measured by ground-based instruments and satellites sensors. Sun photometers in Aerosol RObotic NETwork (AERONET) are the main ground-based instruments that can observe AOD every 15 min (Holben et al., 1998). The measurements from sun photometers are usually used as the reference data to validate the satellite AOD retrievals (Tao et al., 2017a, 2017b; Wei et al., 2018). Satellite sensors have been demonstrated promising accuracies in the retrieval of AOD (Levy et al., 2013; Zhang et al., 2016b). In recent years, many satellite sensors are launched to monitor the global aerosol loadings (Wang et al., 2003; Zhang et al., 2011; Pang et al., 2018). Himawari-8 is a new-generation of geostationary meteorological satellite. The primary instruments aboard Himawari-8 is Advanced Himawari Imager (AHI), which is a 16 channels sensor to capture visible and infrared images over East Asia, Southeast Asia, and Oceania. The new-generation

\* Corresponding author.

\*\* Corresponding author.

E-mail address: [zhaoyang.zhang@connect.polyu.hk](mailto:zhaoyang.zhang@connect.polyu.hk) (Z. Zhang).

geostationary satellite has higher radiometric, spectral, and spatial resolution than those previously available in geostationary orbit (Bessho et al., 2016; Takeuchi, 2016). The sensor can be used to retrieve aerosol properties at high temporal resolution, which is very useful to inverse modelling of emissions and derive the high temporal surface particle matters (Yumimoto et al., 2016).

China has been suffering severe aerosol pollution due to the large energy combustion from industries and vehicles (Zhang et al., 2015, 2018). What is more, naturally dust and smoke from biomass burning also occurs in China. Therefore, hazy days occur frequently in China, especially in Beijing. The maximum PM<sub>2.5</sub> mass concentrations in Beijing exceed 500 μgm<sup>-3</sup> in January 2013 (Tao et al., 2014). High temporal resolution of AOD is benefit for improving the estimation of PM<sub>2.5</sub> mass concentrations and tracking the transport of atmospheric pollution. Most of the satellite aerosol algorithms are based on look up tables, which are created by using radiative transfer models (Li et al., 2009; Choi et al., 2016). Deep blue (DB) and dark target (DT) algorithm are used to derive AOD for Moderate Resolution Imaging Spectroradiometer (MODIS) with look up tables. The expected errors of DT and DB AOD over land are within ± 0.05 ± 0.15 × AOD (Levy et al., 2013) and ± 0.03 ± 0.2 × AOD (Sayer et al., 2013), respectively. Bilal et al. (2013) developed a simplified aerosol algorithm using MODIS surface reflectance and AERONET AOD for MODIS without look up tables and the algorithm has a good agreement with ground-based observations. However, they ignored the diffuse transmittance for simplification and this could induce large error for high AOD (> 2). In this paper, a novel aerosol algorithm is developed to retrieve the hourly AOD from AHI, which can be used for high aerosol loadings. The paper is organized as follows. Descriptions of the data, methodology are outlined in Section 2. In Section 3, the SARAHI retrieval AOD are presented. Section 4 summarizes the conclusions.

## 2. Data and method

### 2.1. JAXA AHI data

Himawari-8 was launched in October 2014 and carried a new payload called the AHI. This satellite is a geostationary weather satellite and can provide aerosol parameters every 10 min over East Asia, Southeast Asia, part of South Asia, and Oceania. It is one of the few sensors that can provide diurnal variability of AOD. Hourly daytime (3:00–7:00 UTC) AHI L1 data in January 2016 is used in this paper. AHI L1 gridded data (NetCDF4 format) for full-disk generated by Japan Aerospace Exploration Agency (JAXA) provides albedo data from band 1 to band 6 (Table 1) (Bessho et al., 2016), which can cover the eastern China. Band 2 was used to retrieval AOD. The spatial resolution of the JAXA Himawari L1 gridded data is at 5 km × 5 km. The L2ARP2.0 data are also used in this paper to compare with the new AHI aerosol retrievals. The Aerosol Optical Depth (AOD) product at 500 nm is retrieved using the second lowest land surface reflectance in a month and calculated sea surface reflectance based on the model developed by Cox and Munk (1954) and wind speed from JMA global analysis (GANAL) data (Ishihara et al., 2006). The aerosol model in the aerosol retrieval algorithm of AHI was made up of external mixture of fine and coarse aerosol particles. Fine aerosol model was based on the average properties of the fine mode for category 1–6 by Omar et al. (2005), which provide the global aerosol models using AERONET (Holben et al., 1998) measurements. For the coarse aerosol model, the external mixture of the pure marine aerosol on the basis of the model illustrated by Sayer

**Table 1**  
Detailed parameters of AHI imager in visible and near-infrared wavelength.

Wavelength (μm)	0.47	0.51	0.64	0.86	1.6	2.3
Central wavelength (μm)	0.47063	0.51	0.63914	0.8567	1.6101	2.2568
Band number	1	2	3	4	5	6

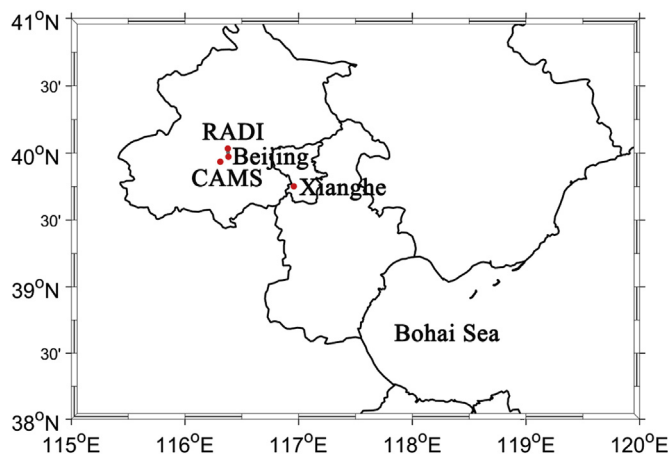


**Fig. 1.** AERONET stations used in this study.

et al. (2012) and a dust model based on the coarse model of category 1 (dust) illustrated by Omar et al. (2005) was adopted in the algorithm. The detailed information about the L2ARP2.0 AOD can be found in Yoshida et al. (2018) and Kikuchi et al. (2018).

### 2.2. AERONET data

AERONET station measurements used in this study are obtained from AERONET website (<https://aeronet.gsfc.nasa.gov/>). The AERONET project is a federation of ground-based sun photometers initiated by NASA (Holben et al., 1998). It can provide aerosol information every 15 min in cloudless day. AERONET AOT data have higher accuracy of < ± 0.01 for aerosol retrieval for wavelengths longer than 440 nm and < ± 0.02 for shorter wavelengths without cloud contamination (Holben et al., 1998). However, the bias may increase to 0.031–0.060 under thin cirrus cloud contamination (Chew et al., 2011). AERONET inversion algorithm also provides the aerosol optical properties, such as single scattering albedo and asymmetry (Dubovik et al., 2002). Fig. 1 shows the AERONET stations used in this study. AERONET Version 3 level 2.0 aerosol data are used in this study. In this paper, Beijing (39.976° N, 116.381° E) AERONET station is adopted to develop the aerosol algorithm. Beijing\_RADI (40.005° N, 116.379° E), Beijing\_CAMS (39.933° N, 116.317° E), and Xianghe (39.753° N, 116.961° E) AERONET sites in January 2016 are used to validate the SARAHI aerosol retrievals.

### 2.3. Radiative transfer model

The basic radiative transfer equation in plane-parallel atmospheres consists of two differential equations, including upward radiant flux and downward radiant flux. The equations are as follows:

$$\frac{dF^{\uparrow}(\tau)}{d\tau} = -m_1(k + \sigma\Gamma_1(\tau))F^{\uparrow}(\tau) + m_2(\tau)\sigma\Gamma_2(\tau)F^{\downarrow}(\tau) \tag{1}$$

$$-\frac{dF^{\downarrow}(\tau)}{d\tau} = -m_2(k + \sigma\Gamma_2(\tau))F^{\downarrow}(\tau) + m_1(\tau)\sigma\Gamma_1(\tau)F^{\uparrow}(\tau) \tag{2}$$

Where

$$m_1(\tau) = \frac{\int_0^{2\pi} I_1(\tau, r')d\Omega}{\int_0^{2\pi} I_1(\tau, r')\cos\theta_0 d\Omega}$$

$$m_2(\tau) = \frac{\int_0^{2\pi} I_2(\tau, r')d\Omega}{\int_0^{2\pi} I_2(\tau, r')\cos\theta_0 d\Omega}$$

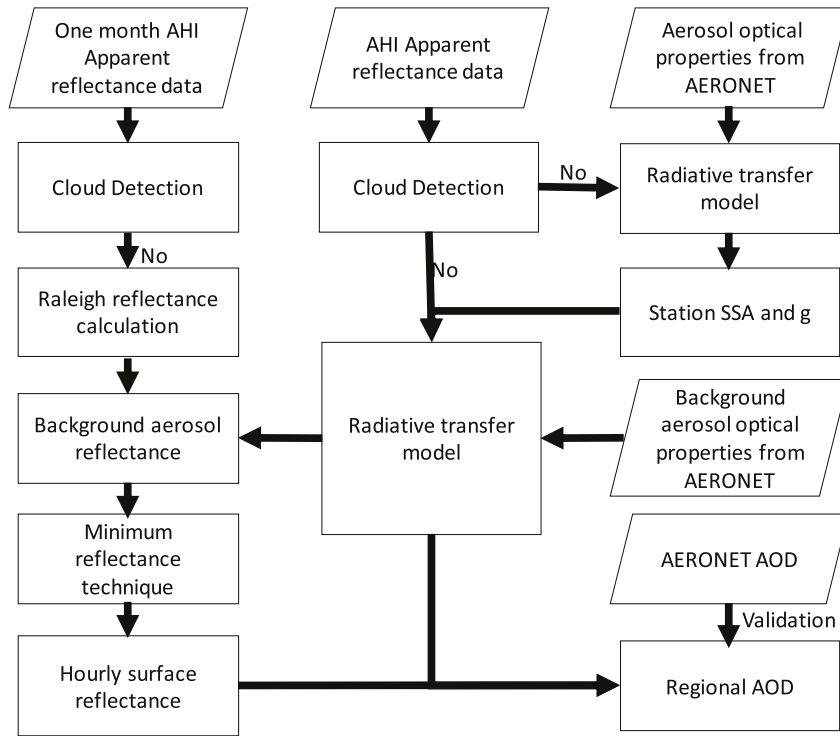


Fig. 2. Flowchart of the aerosol retrieval algorithm used in this study.

$$\Gamma_1(\tau) = \frac{\int_0^{2\pi} I_1(\tau, r')\beta_1(r')d\Omega}{\int_0^{2\pi} I_1(\tau, r')d\Omega}$$

$$\Gamma_2(\tau) = \frac{\int_0^{2\pi} I_2(\tau, r')\beta_2(r')d\Omega}{\int_0^{2\pi} I_2(\tau, r')d\Omega}$$

$$\beta_1(r') = \frac{1}{4\pi} \int_0^{2\pi} \gamma_1(\tau, r', r)d\Omega$$

$$\beta_2(r') = \frac{1}{4\pi} \int_0^{2\pi} \gamma_2(\tau, r', r)d\Omega$$

$$I_1(\tau, r) = I(\tau, r)$$

$$I_2(\tau, r) = I(\tau, -r)$$

$$\gamma_1(\tau, r', r) = \gamma(\tau, -r', r)$$

$$\gamma_2(\tau, r', r) = \gamma(\tau, r', -r)$$

$r'$  represents for the direction of the incident radiation.  $\theta_0$  and  $\theta$  is the solar zenith angle and sensor zenith angle, respectively.  $\phi_0$  and  $\phi$  represent the solar azimuth angle and sensor azimuth angle, respectively.  $r$  represents the direction of the reflected radiation.  $\Omega$  represent solid angle.  $k$  is the absorption coefficient, and  $\sigma$  is the scattering coefficient. In the equation,  $\tau$  consists of molecular scattering ( $\tau_m$ ) and scattering by aerosol particles ( $\tau_a$ ).

The following boundary conditions for the upward and downward fluxes at the top and bottom of the atmosphere are as following.

$$F^{\downarrow}(\tau = \tau_0) = E_0^{\lambda} \cos\theta_0 \quad (3)$$

$$F^{\uparrow}(\tau = 0) = R'F^{\downarrow}(\tau = 0) \quad (4)$$

$E_0^{\lambda}$  represents the extraterrestrial solar irradiance. The relationship between surface reflectance  $R$  and TOA reflectance  $R'$  can be calculated (Mei et al., 2013) as followings.

$$R = \frac{(1 - R'M_1)e^{\rho_1\tau} + (R'M_2 - 1)e^{\rho_2\tau}}{(1 - R'M_1)M_2e^{\rho_1\tau} + (R'M_2 - 1)M_1e^{\rho_2\tau}} \quad (5)$$

Where

$$M_1 = \frac{m_1(1 - \varpi) + m_1\varpi\Gamma + \rho_1}{m_2\varpi\Gamma}$$

$$M_2 = \frac{m_1(1 - \varpi) + m_1\varpi\Gamma + \rho_2}{m_2\varpi\Gamma}$$

$$\rho_1 = \frac{(m_2 - m_1)(1 - \varpi + \varpi\Gamma) + \sqrt{(m_1 - m_2)^2(1 - \varpi + \varpi\Gamma)^2 + 4m_1m_2(1 - \varpi)(1 - \varpi + 2\varpi\Gamma)}}{2}$$

$$\rho_2 = \frac{(m_2 - m_1)(1 - \varpi + \varpi\Gamma) - \sqrt{(m_1 - m_2)^2(1 - \varpi + \varpi\Gamma)^2 + 4m_1m_2(1 - \varpi)(1 - \varpi + 2\varpi\Gamma)}}{2}$$

$$m_1 = m_1(\tau) = 2, \quad m_2 = m_2(\tau) = \sec\theta,$$

$$\Gamma = \Gamma(\tau) = \frac{\tau_m}{2\tau} + \frac{\tau_a(1-g)}{2g\tau} \left( \frac{1+g}{(1+g^2)^{0.5}} - 1 \right), \quad \tau_m = 0.00864\lambda^{(-3.916-0.074\lambda-0.05/\lambda)}$$

$G$  is asymmetry factor and  $\varpi$  is the single scattering albedo.

#### 2.4. Inverse problem

A simplified aerosol retrieval algorithm for AHI is developed by using the radiative transfer model in Section 2.3. The new algorithm runs without look up table. Fig. 2 shows the flowchart of the simplified aerosol retrieval algorithm. The cloudy regions in the aerosol retrieval algorithm are masked by the beta JAXA AHI cloud products (Ishida and Nakajima, 2009; Ishida et al., 2011). The unknown parameters in Equation (5) are surface reflectance, single scattering albedo, asymmetry factor and AOD.

For surface reflectance estimation, cloud is removed from one-month AHI apparent reflectance data. The clear-sky pixels are corrected to derive the Rayleigh-corrected reflectance by using the approximation for Rayleigh scattering (Liang, 2004). We also assumed that changes in

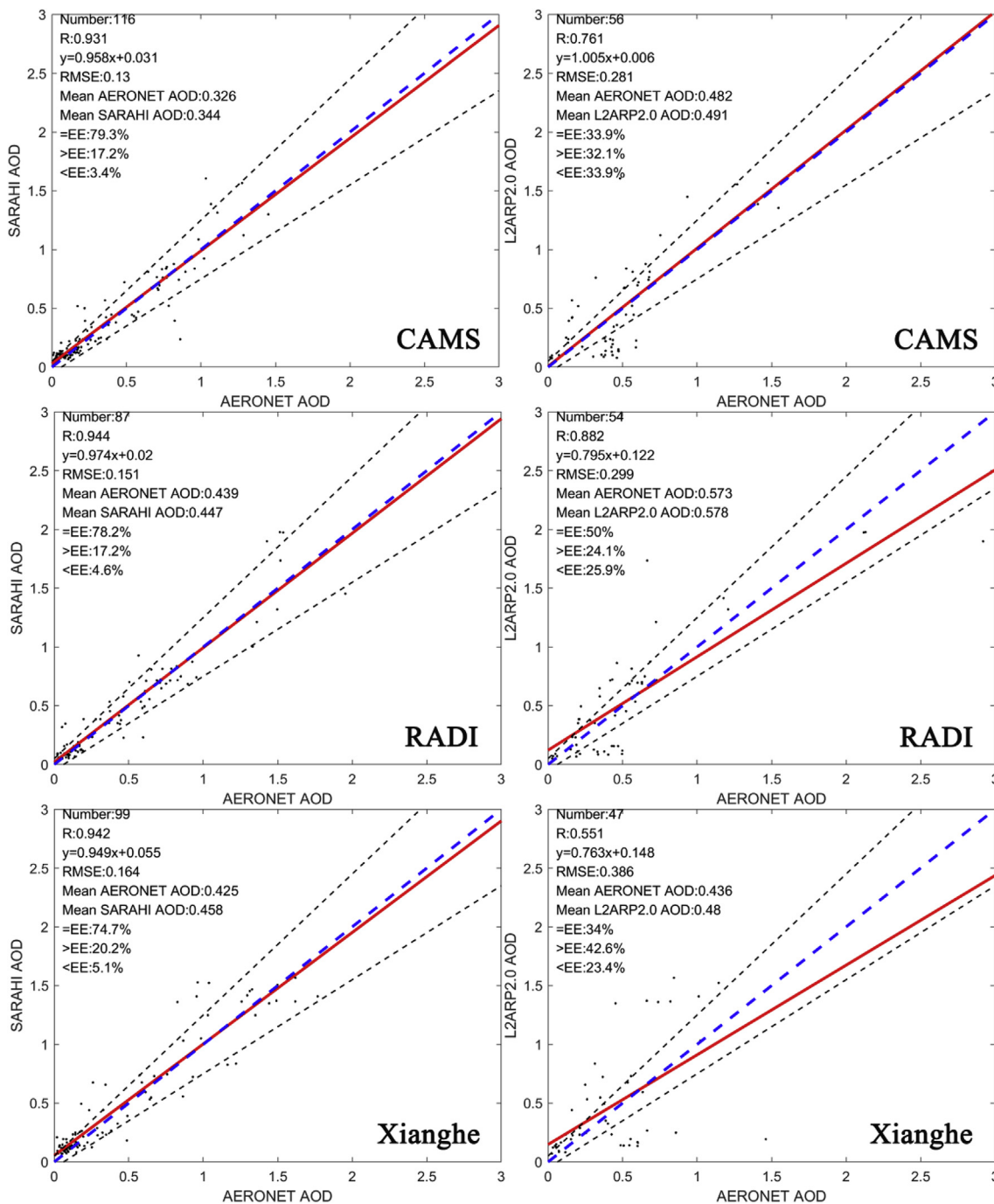


Fig. 3. Scatter plots of AERONET AOD, SARAH1 AOD, and L2ARP2.0 AOD.

surface reflectance are insignificant in one-month period (Li et al., 2013). What is more, the minimum apparent reflectance has the lowest aerosol impact. The single scattering albedo, asymmetry factor, and lowest AOD, in January 2016 is extracted from Beijing AERONET site. One-month Rayleigh-corrected reflectance data is then corrected using the background aerosol reflectance. The hourly surface reflectance is obtained from one-month apparent data in every hour by repeating the process.

Single scattering albedo, asymmetry factor and AOD are the remaining unknown parameters in Equation (5). Aerosol optical properties from Beijing AERONET sites are as input in the equation. Then, the single scattering albedo and asymmetry factor for JAXA AHI aerosol retrieval are derived by varying the single scattering albedo and asymmetry factor until left and right in the equation is equal or

minimum difference is calculated using fixed point iteration method (Kelley, 1995). The calculated single scattering albedo and asymmetry factor are used as input in Equation (5) to retrieve regional AOD. Fixed single scattering albedo and asymmetry factor are assumed in a relative small regions (Bilal et al., 2013). The new algorithm was named SARAH1 for short. The other three AERONET sites are used to validate the SARAH1 AOD.

### 3. Results and analysis

#### 3.1. Validation with AERONET observations

The SARAH1 AOD and L2ARP2.0 AOD were validated with Beijing RAD1, Beijing CAMS, and Xianghe AOD (Fig. 3). In Fig. 3, the blue

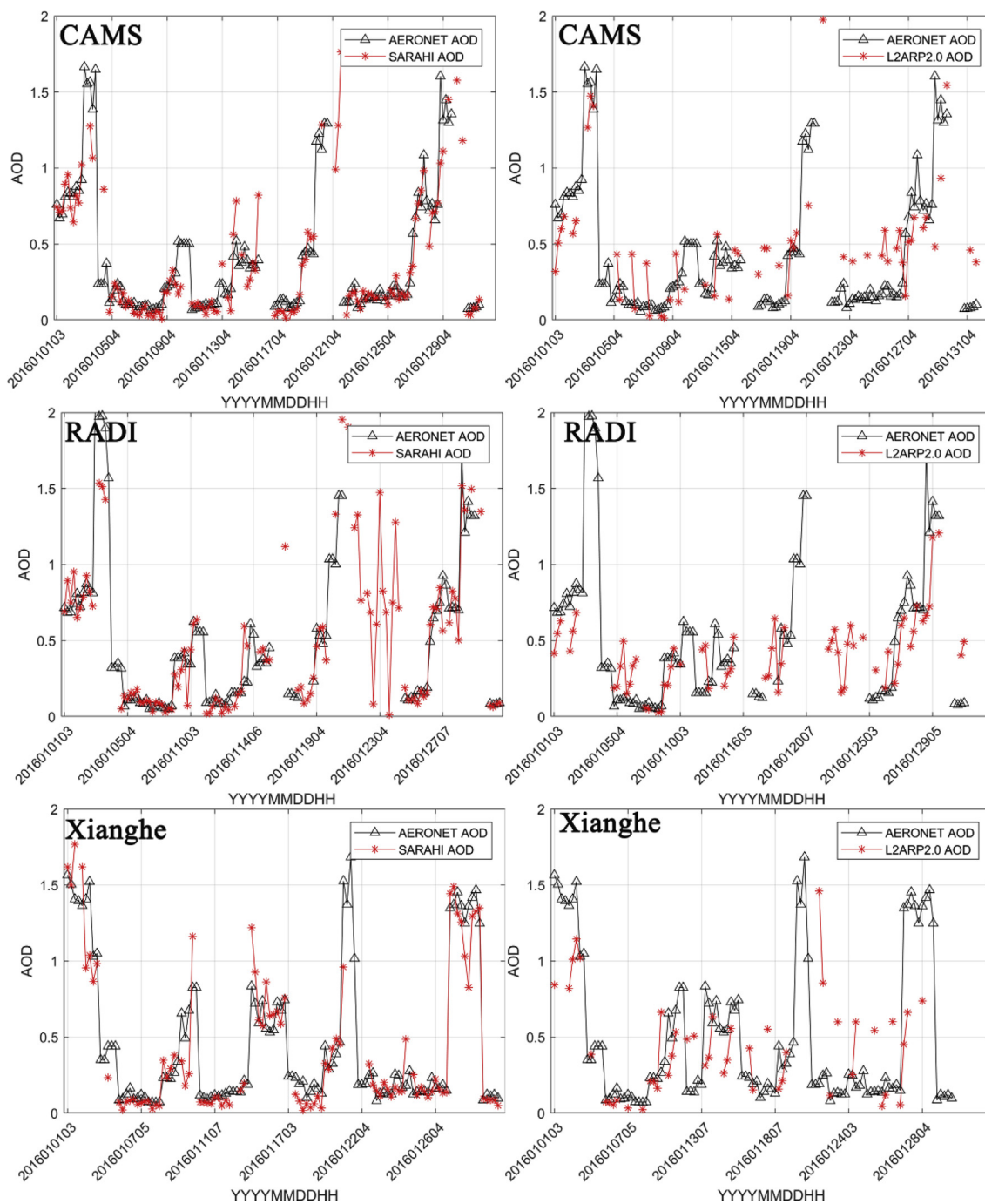


Fig. 4. Times series of AERONET AOD, SARAH1 AOD, and L2ARP2.0 AOD.

dotted lines represent 1:1 line, red solid lines are the regression lines, and black dotted lines are the expected error lines. 136, 87, and 99 collections are obtained for Beijing\_CAMS, Beijing\_RADI, and Xianghe sites, respectively. The SARAH1 AOD retrievals agree well with AERONET AOD at Beijing\_CAMS. The SARAH1 AOD shows a high correlation (0.925) with AERONET AOD with an RMSE of 0.134. There are 73.5% of AOD retrievals falling in the expected error lines at Beijing\_CAMS station. In Beijing\_RADI site, the SARAH1 AOD retrievals also show good consistency with AERONET measurements. The correlation reaches at 0.944 and the 78.2% of AOD retrievals fall within the expected error line. There is also high consistency between AOD retrievals and AERONET AOD observations (0.942) at Xianghe AERONET site and low RMSE errors of 0.164. There are 74.7% of AOD retrievals within the expected error lines for this station. The results show that

high correlation from 0.925 to 0.945 is observed with small RMSE of 0.134–0.164, indicating the algorithm is robust and can retrieve AOD with more accuracy than the JAXA AHI aerosol products.

Scatter plots of L2ARP2.0 AOD and AERONET AOD are also illustrated in Fig. 3. Low correlation of 0.488 (Number = 56) with large RMSE (0.281) is observed in Beijing\_CAMS site. 32.1% of the L2ARP2.0 AOD retrievals are greater than AERONET AOD measurements and 33.9% of them is underestimated at Beijing\_CAMS site. For the Beijing\_RADI site, the correlation is about 0.882. However, the slope is about 0.795 with large RMSE (0.299). There is ~50% of L2ARP2.0 AOD within the expected error lines. Poor consistency between L2ARP2.0 AOD and AERONET AOD observations is also shown in Xianghe AERONET site. The correlation is only about 0.551. 66% of L2ARP2.0 AOD observations fall out of the expected lines and the RMSE is about

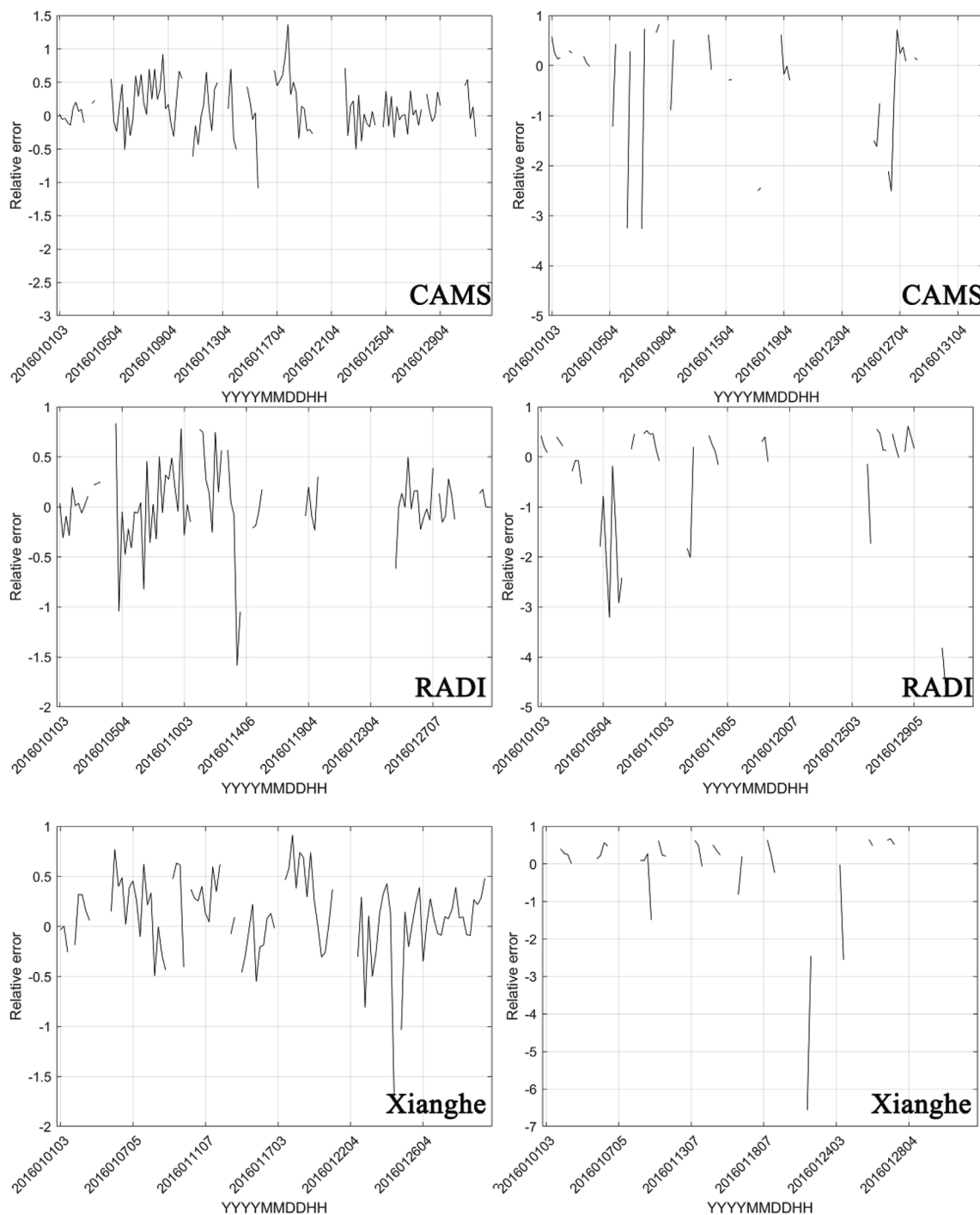


Fig. 5. Relative errors of SARAH1 AOD, and L2ARP2.0 AOD at Beijing\_CAMS, Beijing\_RADI, and Xianghe AERONET sites.

0.386. The accuracy of the L2ARP2.0 AOD is affected by aerosol model and surface reflectance. Further research about the problem of L2ARP2.0 AOD will be conducted.

### 3.2. Time series analysis of AOD

Fig. 4 shows the times series of AERONET AOD, SARAH1 AOD, and L2ARP2.0 AOD. It is apparent that the SARAH1 AOD measurements agree well with AERONET AOD and they can reflect the temporal variations of aerosol loadings very well for all these three AERONET sites. For the Beijing\_CAMS site, L2ARP2.0 AOD cannot capture the variations of AOD. For Beijing\_RADI and Xianghe AERONET sites,

L2ARP2.0 AOD can generally reflect the variation of aerosol. However, the low AOD is overestimated in Beijing\_CAMS station and high AOD is underestimated in Xianghe station. Relative error  $((AOD_{AERONET} - AOD_{AHI}) / AOD_{AERONET})$  of SARAH1 AOD and L2ARP2.0 AOD at Beijing\_CAMS, Beijing\_RADI, and Xianghe sites is shown in Fig. 5. Most of the relative errors of SARAH1 AOD lie between  $-1$  and  $1$ , and these errors are centered on  $0$ . The maximum relative errors of SARAH1 AOD are about  $1.4$ ,  $-1.6$ , and  $-1.6$  in Beijing\_CAMS, Beijing\_RADI, and Xianghe, respectively. For L2ARP2.0 AOD retrievals, the relative errors lie between  $-7$  and  $1$ . The maximum relative error of L2ARP2.0 AOD at Beijing\_CAMS, Beijing\_RADI, and Xianghe is about  $-3.2$ ,  $-3.1$ , and  $-6.6$ , respectively. The AOD at Xianghe and RADI at 4 in January 27,

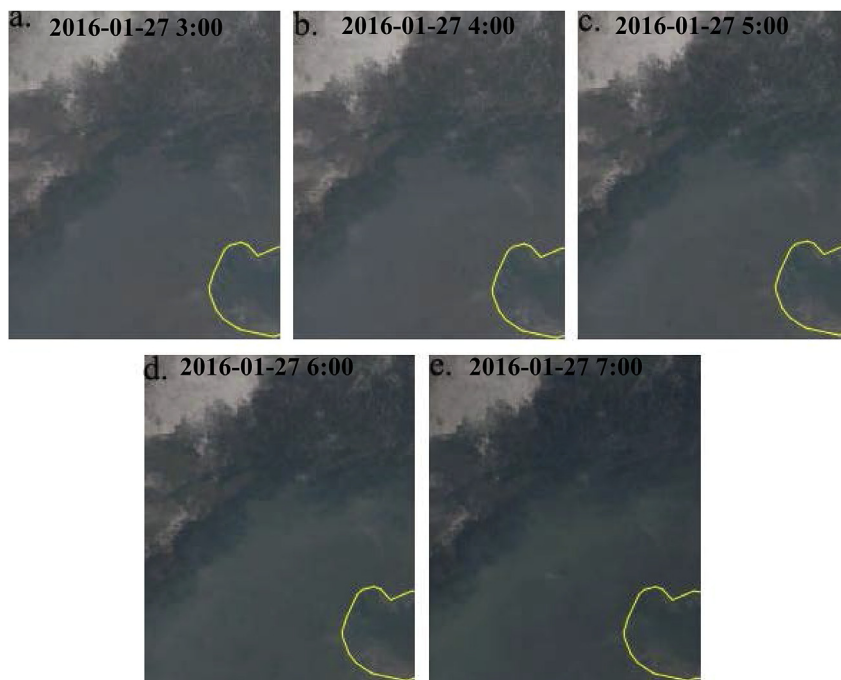


Fig. 6. True color images during 3:00–7:00 on January 27, 2016. (For interpretation of the references to color in this figure legend, the reader is referred to the Web version of this article.)

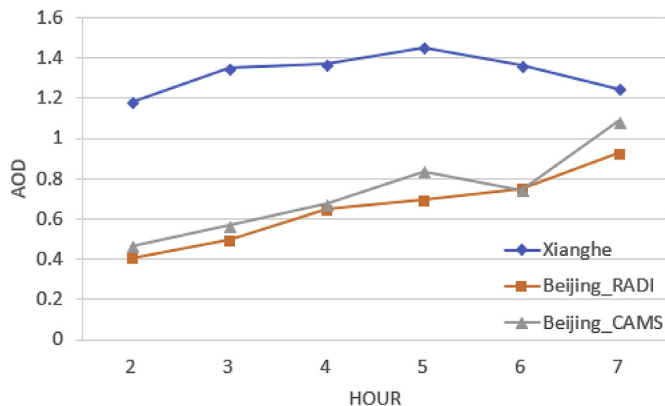


Fig. 7. Time series of AOD at Beijing\_CAMS, Beijing\_RADI, and Xianghe AERONET sites.

2016 from our algorithm and aerosol product are missing. This is caused by the beta JAXA AHI cloud products in the aerosol algorithm. The analysis indicates that SARAHI AOD has better ability to retrieve AOD and it is superior to JAXA AHI aerosol products.

### 3.3. Spatial distribution of AOD retrievals in haze weather

Fig. 6 shows the true color images and Fig. 8 represents spatial distribution of AOD from Himawari. According to Fig. 6a, there is a high aerosol layer locating in the east of Yanshan Mountain from 3:00 to 7:00 on January 27, 2016. Beijing\_CAMS and Beijing\_RADI are in the urban center of Beijing. Xianghe site lies in a suburban area 75 km to the east of Beijing. High AOD at about 2:00 was measured in Xianghe AERONET site (1.180 at 440 nm), while the AOD at 440 nm in Beijing\_RADI and Beijing\_CAMS was 0.407 and 0.466, respectively (Fig. 7). Due to the influence of wind, the aerosol layer seems to steadily be in the northwest direction. Therefore, higher AOD at Beijing\_RADI and Beijing\_CAMS is shown during 3:00–7:00. Fig. 8 shows the spatial distribution of AOD from L2ARP2.0. The direction of movement of the aerosol layer from L2ARP2.0 is consistent with ground-based

measurements. However, there are many pixels missing in the L2ARP2.0. The spatial distribution of L2ARP2.0 AOD is noncontiguous and there are many high values under low background AOD. The spatial distribution of SARAHI AOD was shown in Fig. 9. The figure shows that the aerosol layer moves to Beijing direction. The maximum AOD of the heavy aerosol layer was about 2. Part of the heavy aerosol layer dissipated at 7:00. The analysis indicates that the SARAHI algorithm is capable for retrieving accurate AOD.

### 4. Conclusion

A novel simplified aerosol retrieval algorithm for Himawari-8 (SARAHI) is proposed using a modified radiative transfer model without lookup table. Fixed regional single scattering albedo and asymmetry factor is assumed. Beijing\_CAMS, Beijing\_RADI, and Xianghe AERONET sites are used to validate the hourly SARAHI AOD. SARAHI AOD retrievals from new algorithm show better consistency with AERONET measurements than L2ARP2.0 AOD. The correlation coefficient between AERONET AOD measurements and AHI AOD retrievals from simplified method exceeds 0.92 with the RMSE of 0.134–0.164, while the correlation coefficient for L2ARP2.0 AOD is smaller than 0.882 with RMSE of 0.281–0.386. Time series of AOD analysis demonstrates that the SARAHI AOD has similar temporal variation of AOD with those measurements from three AERONET sites. The SARAHI AOD can capture the spatial-temporal AOD in heavy polluted weather. The analysis indicates that the new algorithm has better agreement with AERONET measurements than L2ARP2.0 AOD over Beijing. The results in this study can be used to fully understand the effect of aerosol on climate studies and estimating the surface particles matter concentrations.

### Acknowledgments

This work was supported by the Strategic Priority Research Program of the Chinese Academy of Sciences (Grant No. XDA19040201). Z. Zhang was also supported by projects of the Natural Science Foundation of Zhejiang Province (Grant No. LQ18D010004) and National Science Foundation of China (Grant No. 41801258). The author would like to

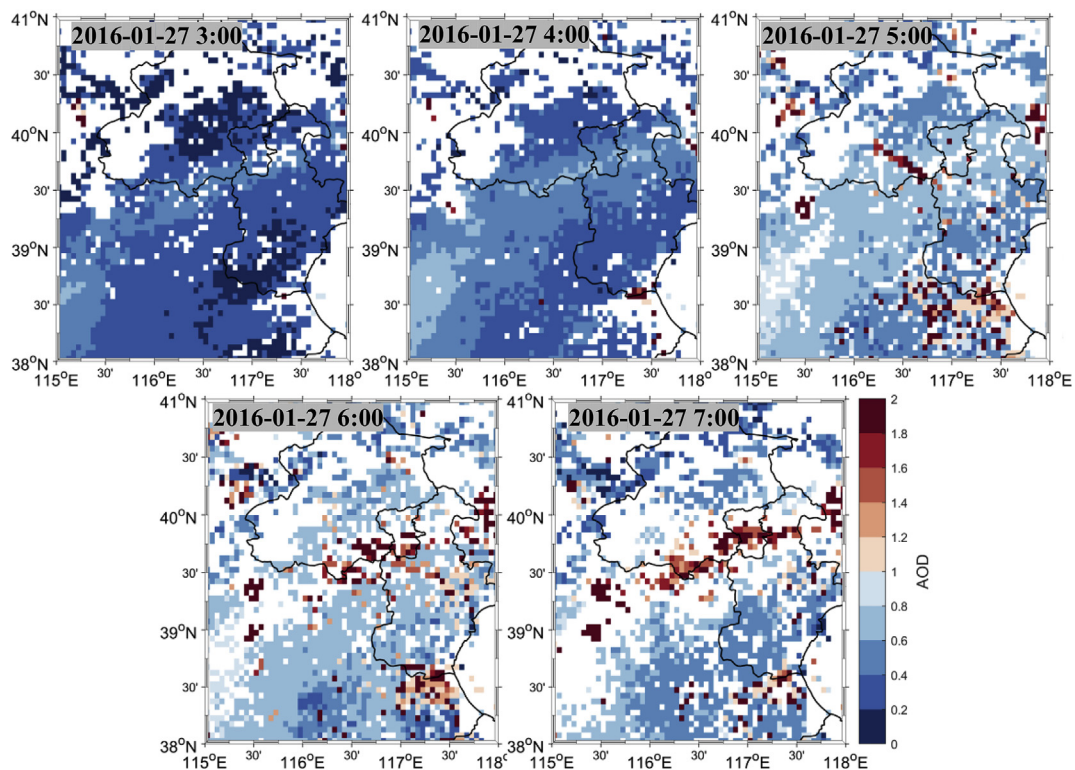


Fig. 8. Spatial distribution of AOD from L2ARP2.0 AOD during 3:00–7:00 (UTC) on January 27, 2016.

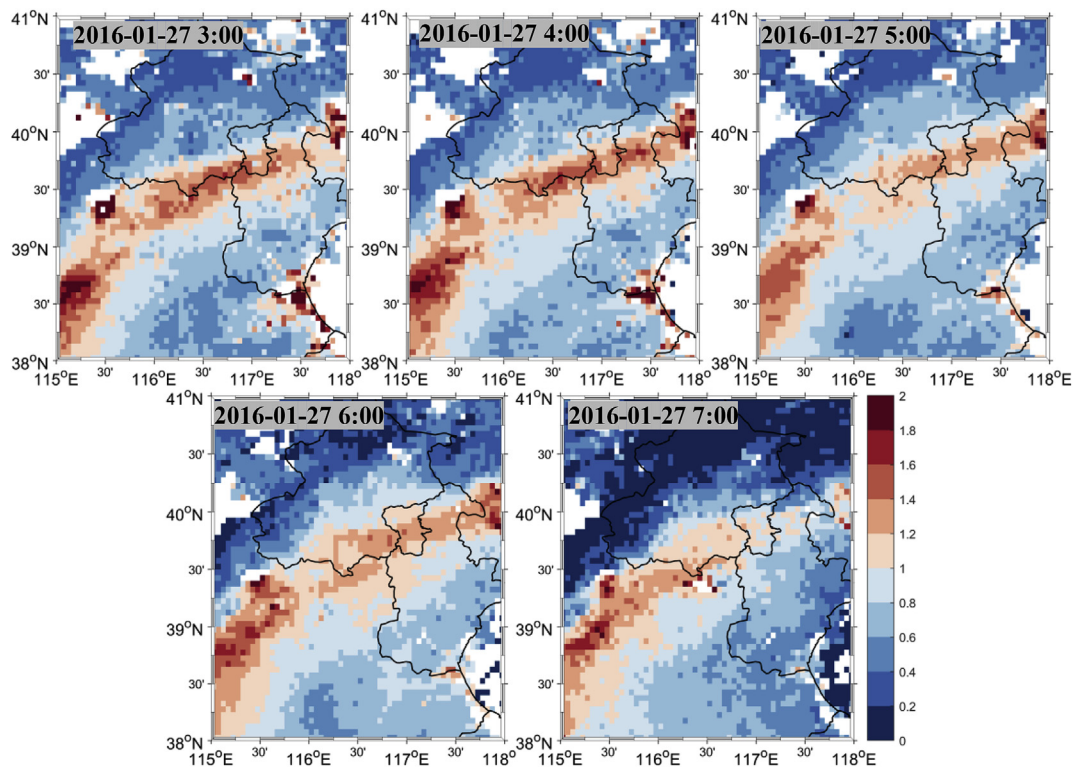


Fig. 9. Spatial distribution of SARAHI AOD during 3:00–7:00 (UTC) on January 27, 2016.

thank the editor and the reviewers for their useful comments and suggestions. Himawari-8 L1 reflectance used in this paper were supplied by the P-Tree System, Japan Aerospace Exploration Agency. Research product of aerosol and cloud properties (produced from Himawari-8) that was used in this paper was derived by the algorithm

developed by Japan Aerospace Exploration Agency and National Institute for Environmental Studies. The authors would like to thank the team of AERONET and JAXA for their hard work.

## Appendix A. Supplementary data

Supplementary data related to this article can be found at <https://doi.org/10.1016/j.atmosenv.2018.11.023>.

## References

- Bessho, K., Date, K., Hayashi, M., Ikeda, A., Imai, T., Inoue, H., Kumagai, Y., Miyakawa, T., Murata, H., Ohno, T., Okuyama, A., Oyama, R., Sasaki, Y., Shimazu, Y., Shimoji, K., Sumida, Y., Suzuki, M., Taniguchi, H., Tsuchiyama, H., Uesawa, D., Yokota, H., Yoshida, R., 2016. An introduction to Himawari-8/9 - Japan's new-generation geostationary meteorological satellites. *J. Meteorol. Soc. Jpn. Ser. II* 94, 151–183.
- Bilal, M., Nichol, J.E., Bleiweiss, M.P., Dubois, D., 2013. A Simplified high resolution MODIS Aerosol Retrieval Algorithm (SARA) for use over mixed surfaces. *Remote Sens. Environ.* 136, 135–145.
- Chen, C., Zhao, B., Weschler, C.J., 2012. Indoor exposure to “outdoor PM10”: assessing its influence on the relationship between PM10 and short-term mortality in US cities. *Epidemiology* 23, 870–878.
- Chew, B.N., Campbell, J.R., Reid, J.S., Giles, D.M., Welton, E.J., Salinas, S.V., Liew, S.C., 2011. Tropical cirrus cloud contamination in sun photometer data. *Atmos. Environ.* 45, 6724–6731.
- Choi, M., Kim, J., Lee, J., Kim, M., Park, Y.J., Jeong, U., Kim, W., Hong, H., Holben, B., Eck, T.F., Song, C.H., Lim, J.H., Song, C.K., 2016. GOCI Yonsei aerosol retrieval (YAER) algorithm and validation during the DRAGON-NE Asia 2012 campaign. *Atmos. Meas. Tech.* 9, 1377–1398.
- Cox, C.S., Munk, W.H., 1954. Statistics of the sea surface derived from sun glitter. *J. Mar. Res.* 13, 198–227.
- Dubovik, O., Holben, B., Eck, T.F., Smirnov, A., Kaufman, Y.J., King, M.D., Tanre, D., Slutsker, I., 2002. Variability of absorption and optical properties of key aerosol types observed in worldwide locations. *J. Atmos. Sci.* 59, 590–608.
- Field, C.B., Barros, V.R., Mach, K., Mastrandrea, M., 2014. Climate Change 2014: Impacts, Adaptation, and Vulnerability. Working Group II Contribution to the IPCC 5th Assessment Report-technical Summary. pp. 1–76.
- Hinds, W.C., 1999. *Aerosol Technology: Properties, Behavior, and Measurement of Airborne Particles* (2nd).
- Holben, B.N., Eck, T.F., Slutsker, I., Tanre, D., Buis, J.P., Setzer, A., Vermote, E., Reagan, J.A., Kaufman, Y.J., Nakajima, T., Lavenue, F., Jankowiak, I., Smirnov, A., 1998. AERONET - a federated instrument network and data archive for aerosol characterization. *Remote Sens. Environ.* 66, 1–16.
- Ishida, H., Nakajima, T.Y., 2009. Development of an unbiased cloud detection algorithm for a spaceborne multispectral imager. *J. Geophys. Res. Atmos.* 114 (n/a-n/a).
- Ishida, H., Nakajima, T.Y., Yokota, T., Kikuchi, N., Watanabe, H., 2011. Investigation of GOSAT TANSO-CAI cloud screening ability through an intersatellite comparison. *J. Appl. Meteorol. Climatol.* 50, 1571–1586.
- Ishihara, M., Kato, Y., Abo, T., Kobayashi, K., Izumikawa, Y., 2006. Characteristics and performance of the operational wind profiler network of the Japan Meteorological Agency. *J. Meteorol. Soc. Jpn. Ser. II* 84, 1085–1096.
- Kelley, C., 1995. *Iterative Methods for Linear and Nonlinear Equations*. Society for Industrial and Applied Mathematics.
- Kikuchi, M., Murakami, H., Suzuki, K., Nagao, T.M., Higurashi, A., 2018. Improved hourly estimates of aerosol optical thickness using spatiotemporal variability derived from Himawari-8 geostationary satellite. *IEEE T Geosci Remote* 56, 3442–3455.
- Levy, R.C., Mattoo, S., Munchak, L.A., Remer, L.A., Sayer, A.M., Patadia, F., Hsu, N.C., 2013. The Collection 6 MODIS aerosol products over land and ocean. *Atmos. Meas. Techn.* 6, 2989–3034.
- Li, S.S., Chen, L., Zheng, F., Han, D., Wang, Z., 2009. Design and application of haze optic thickness retrieval model for Beijing olympic games. In: *Geoscience and Remote Sensing Symposium, 2009. IEEE International, IGARSS 2009*, pp. II-507-II-510.
- Li, S.S., Chen, L.F., Xiong, X.Z., Tao, J.H., Su, L., Han, D., Liu, Y., 2013. Retrieval of the haze optical thickness in North China plain using MODIS data. *IEEE T Geosci Remote* 51, 2528–2540.
- Liang, S., 2004. *Quantitative Remote Sensing of Land Surfaces*. Wiley-Interscience.
- Mei, L.L., Xue, Y., de Leeuw, G., von Hoyningen-Huene, W., Kokhanovsky, A.A., Istomina, L., Guang, J., Burrows, J.P., 2013. Aerosol optical depth retrieval in the Arctic region using MODIS data over snow. *Remote Sens. Environ.* 128, 234–245.
- Omar, A.H., Won, J.G., Winker, D.M., Yoon, S.C., Dubovik, O., McCormick, M.P., 2005. Development of global aerosol models using cluster analysis of Aerosol Robotic Network (AERONET) measurements. *J. Geophys. Res. Atmos.* 110, D10S14.
- Pang, J., Liu, Z., Wang, X., Bresch, J., Ban, J., Chen, D., Kim, J., 2018. Assimilating AOD retrievals from GOCI and VIIRS to forecast surface PM2.5 episodes over Eastern China. *Atmos. Environ.* 179, 288–304.
- Pope, C.A., Ezzati, M., Dockery, D.W., 2009. Fine-particulate air pollution and life expectancy in the United States. *N. Engl. J. Med.* 360, 376–386.
- Sayer, A.M., Hsu, N.C., Bettenhausen, C., Jeong, M.J., 2013. Validation and uncertainty estimates for MODIS Collection 6 “Deep Blue” aerosol data. *J. Geophys. Res. Atmos.* 118, 7864–7872.
- Sayer, A.M., Smirnov, A., Hsu, N.C., Holben, B.N., 2012. A pure marine aerosol model, for use in remote sensing applications. *J. Geophys. Res.* 117.
- Schwartz, J., Neas, L.M., 2000. Fine particles are more strongly associated than coarse particles with acute respiratory health effects in schoolchildren. *Epidemiology* 11, 6–10.
- Takeuchi, W., 2016. Assessment of geometric errors of Advanced Himawari-8 Imager (AHI) over one year operation. In: *IOP Conference Series: Earth and Environmental Science*. IOP Publishing.
- Tao, M., Chen, L., Wang, Z., Wang, J., Che, H., Xu, X., Wang, W., Tao, J., Zhu, H., Hou, C., 2017a. Evaluation of MODIS deep blue aerosol algorithm in desert region of east Asia: ground validation and intercomparison. *J. Geophys. Res.: Atmosphere* 122 (10) 357–310,368.
- Tao, M., Wang, Z., Tao, J., Chen, L., Wang, J., Hou, C., Wang, L., Xu, X., Zhu, H., 2017b. How do aerosol properties affect the temporal variation of MODIS AOD bias in eastern China? *Remote Sens-Basel* 9, 800.
- Tao, M.H., Chen, L.F., Xiong, X.Z., Zhang, M.G., Ma, P.F., Tao, J.H., Wang, Z.F., 2014. Formation process of the widespread extreme haze pollution over northern China in January 2013: implications for regional air quality and climate. *Atmos. Environ.* 98, 417–425.
- Wang, J., Christopher, S.A., Brechtel, F., Kim, J., Schmid, B., Redemann, J., Russell, P.B., Quinn, P., Holben, B.N., 2003. Geostationary satellite retrievals of aerosol optical thickness during ACE-Asia. *J. Geophys. Res. Atmos.* 108, 8657.
- Wei, J., Sun, L., Huang, B., Bilal, M., Zhang, Z., Wang, L., 2018. Verification, improvement and application of aerosol optical depths in China Part 1: inter-comparison of NPP-VIIRS and Aqua-MODIS. *Atmos. Environ.* 175, 221–233.
- WHO, 2005. *Air Quality Guidelines Global Update for Europe*. World Health Organization, World Health Organization, WHO Regional Publications, Bonn, Germany.
- Yoshida, M., Kikuchi, M., Nagao, T.M., Murakami, H., Nomaki, T., Higurashi, A., 2018. Common retrieval of aerosol properties for imaging satellite sensors. *J. Meteorol. Soc. Jpn.* 96B, 193–209 (Ser. II advpub).
- Yumimoto, K., Nagao, T.M., Kikuchi, M., Sekiyama, T.T., Murakami, H., Tanaka, T.Y., Ogi, A., Irie, H., Khatri, P., Okumura, H., Arai, K., Morino, I., Uchino, O., Maki, T., 2016. Aerosol data assimilation using data from Himawari-8, a next-generation geostationary meteorological satellite. *Geophys. Res. Lett.* 43, 5886–5894.
- Zhang, H., Lyapustin, A., Wang, Y., Kondragunta, S., Laszlo, I., Ciren, P., Hoff, R.M., 2011. A multi-angle aerosol optical depth retrieval algorithm for geostationary satellite data over the United States. *Atmos. Chem. Phys.* 11, 11977–11991.
- Zhang, Z.Y., Wong, M.S., Campbell, J.R., 2018. Conceptualizing How Severe Haze Events Are Impacting Long-term Satellite-based Trend Studies of Aerosol Optical Thickness over Asia. Springer, Cham.
- Zhang, Z.Y., Wong, M.S., Lee, K.H., 2015. Estimation of potential source regions of PM2.5 in Beijing using backward trajectories. *Atmos. Pollut. Res.* 6, 173–177.
- Zhang, Z.Y., Wong, M.S., Lee, K.H., 2016a. Evaluation of the representativeness of ground-based visibility for analysing the spatial and temporal variability of aerosol optical thickness in China. *Atmos. Environ.* 147, 31–45.
- Zhang, Z.Y., Wong, M.S., Nichol, J., 2016b. Global trends of aerosol optical thickness using the ensemble empirical mode decomposition method. *Int. J. Climatol.* 36, 4358–4372.